PRAMANA — journal of physics

Vol. 84, No. 4
April 2015
pp. 591–608

Characteristics of disintegration of different emulsion nuclei by relativistic ^{28}Si nuclei at 3.7 A GeV

ASHWINI KUMAR[1,*], A PRAKASH[1], ASHOK KUMAR[2], R K JAIN[3] and B K SINGH[1]

[1]High Energy Physics Laboratory, Department of Physics, Banaras Hindu University, Varanasi 221 005, India
[2]Department of Applied Science (Physics), Vidya College of Engineering, Meerut 250 010, India
[3]Department of Physics, Faculty of Humanities, Physics and Mathematical Sciences, Shobhit University, Meerut 250 110, India
*Corresponding author. E-mail: ashwini.physics@gmail.com

MS received 3 January 2014; revised 22 April 2014; accepted 13 May 2014
DOI: 10.1007/s12043-014-0849-8; ***e*Publication:** 29 November 2014

Abstract. An analysis of the data based on 924 inelastic interaction events induced by ^{28}Si nuclei in a nuclear emulsion is presented. The nuclear fragmentation process is studied by analysing the total charge (Q) distribution of the projectile spectators for different emulsion target groups along with the comparison of Monte Carlo Glauber model results. Probability distributions for total disintegrated events as a function of different projectile masses are shown and compared with cascade evaporation model results at same energy per nucleon. Further, mean multiplicities of different charged secondaries for different classes of events are presented and for each event, variation of mean multiplicities as a function of total charge (Q) is also presented. The pseudorapidity distributions and normalized pseudorapidity distributions of the produced charged particles in nucleus–nucleus collisions at 3.7 A GeV are analysed for total disintegration (TD) as well as minimum-bias events.

Keywords. Nuclear emulsion; pseudorapidity; nuclear fragmentation; Monte Carlo Glauber model.

PACS Nos 29.40.Rg; 25.75.−q; 25.70.Mn

1. Introduction

Nucleus–nucleus collisions at relativistic energy have been a subject of immense importance due to its possible connection with critical phenomenon such as phase transition and new/exotic phenomenon predicted by various existing theories [1–4]. In this search, the physics community has devoted much efforts on both the theoretical and experimental fronts and is still in the process of drawing a firm conclusion in this field. Besides this central objective, several other important features of nucleus–nucleus collisions such as particle production [5,6] and fragmentation mechanisms can be studied as

well, to have a better understanding of the dynamics involved in such nuclear collisions. As the colliding heavy ions are rather complicated systems, multiparticle production is still a longstanding unsolved problem which demands a more profound effort to have a clear understanding of the mechanisms involved in these collision processes. In nucleus–nucleus collisions at relativistic energies, most of the energy is deposited in the central region (i.e., the overlapping region of two colliding nuclei), from where the multiple production of newly created particles mainly occur in final state. A fraction of available energy is also transferred to the spectator parts of the two colliding nuclei (i.e., the projectile and the target spectators) leaving nuclear remnants in an excited state. The de-excitation of these excited nuclear remnants into lighter nuclear fragments is known as nuclear fragmentation. The fragmentation of relativistic projectile nucleus is of great significance as it leads to the emission of nucleons and fragments of varying sizes (or masses), allowing us to extract information on the fragmentation mechanism involved in such processes. The main sources of these projectile fragments are nucleons and nucleon clusters formed in these nuclear collisions [7]. Nuclear emulsion technique allows us to simultaneously investigate the produced charged particles as well as projectile fragments in available phase-space. Nuclear emulsion, being a composite system of different embedded nuclei, offers a great advantage to study the nuclear collisions of the same projectile nuclei on different emulsion targets simultaneously, with high accuracy and large acceptance but with rather limited statistics. A lot of experimental and theoretical investigations are being carried out in order to understand the production mechanism of final-state particles produced in nucleus–nucleus collisions at relativistic energies. Various exciting phenomena have been studied by analysing the behaviour of nuclear fragments (helium fragments with charge $Z = 2$ upto projectile fragments with charges $Z \geq 3$) emerged out of the spectator part of the projectile nuclei [8]. Recently, we have studied some general [9] and exciting properties [10] such as limiting fragmentation behaviour of these projectile fragments especially in the case of projectile helium fragments (with charge $Z = 2$) emanated from the nucleus–nucleus collisions.

The main motive of this paper is to analyse the disintegration of relativistic ^{28}Si nuclei with different target nuclei of varying sizes present in nuclear emulsion at 3.7 A GeV. In this paper, we present our extensive analysis of the newly produced charged particles as well as projectile fragments in the nucleus–nucleus collisions at 3.7 A GeV. The characteristics of the projectile spectator fragmentation can be described by the probability distributions of non-interacting projectile spectator charge. Thus, the total charge (the Q value) distribution in ^{28}Si collisions at 3.7 A GeV with different emulsion target groups are shown and compared with the Monte Carlo (MC) Glauber model results. Mean multiplicities of different charged secondary particles are studied with different classes of events and are also investigated with different Q values for centrality dependence in individual events. The conventional way of describing particle production in nucleus–nucleus collisions is to measure the charged particle density in the available pseudorapidity space. Thus, we have analysed the experimental characteristics such as pseudorapidity and normalized pseudorapidity density of charged particles with particular emphasis on total disintegration (TD) of AgBr nuclei induced by ^{28}Si and compared the experimental data with similar characteristics of collisions in minimum-bias events to investigate the differences in the mechanism involved for both the cases.

2. Experimental details

Stacks of NIKFI BR2 nuclear emulsion of $16.9 \times 9.6 \times 0.06$ cm^3 dimension have been exposed horizontally to 3.7 A GeV ^{28}Si beam at Dubna Synchrophasotron with a sensitivity for minimum-ionizing particles of typically 28 grains per 100 μm. Each primary ^{28}Si track has been followed using along-the-track scanning technique having very high detection efficiency on an OLYMPUS BH2 microscope under a magnification of 2250 in order to search for inelastic events. A total of 924 inelastic minimum-bias events were selected for further measurements. According to their ionization, range and velocity, the secondary particles were classified into black (b), grey (g), shower (s) and projectile fragments (PFs) having a charge $Z \geq 2$. Black particles are slow velocity particles with $\beta < 0.3$ having a range less than 3 mm in emulsion and ionization $g > 6g_{\min}$, where $g_{\min}$ is the grain density of the singly-charged particle moving with a velocity close to the initial beam velocity. These are low-energy, multiply-charged fragments and are mainly evaporated particles from the target nuclei. Grey particles have a range greater than 3 mm and ionization $1.4g_{\min} < g \leq 6g_{\min}$. These particles are mainly knocked-out protons from the target nucleus. Both black and grey tracks are target fragments emanating from the emulsion target in its excited state. Shower particles have ionization $g \leq 1.4g_{\min}$ and velocity $\beta > 0.7$. Shower particles are mainly relativistic pions, with a small fraction of K-meson, fast protons and antiprotons. Projectile fragments (PFs) with $Z \geq 2$ have $g \geq 4g_{\min}$, emitted in a narrow forward cone. This forward cone is defined by the critical angle $\theta_c = P_F/P_{beam}$, where P_F is the Fermi momentum of the nucleons inside the projectile nucleus and P_{beam} is the incident beam momentum per nucleon. The calculated value of θ_c is 3.0°. In this experiment, we have taken θ_c to be 5° in order to allow some of the fragments to emerge out in a wider cone such as the helium fragments which are found to have a broader distribution upto $\theta = 5°$ [11]. This will also allow us to have an increased statistics of the sample. The multiplicities of black, grey, shower and projectile fragments are denoted by n_b, n_g, n_s and n_F, respectively.

2.1 *Charge estimation of projectile fragments*

The rate of energy loss of a charged particle passing through matter is directly proportional to the grain density, i.e., the number of grains developed per unit length along the track. Grain density may thus be used directly as a measure of charge when ionization is small. When grain density increases, the adjacent grains become unresolvable under the microscope and form blobs. In this situation, it is very difficult to count grains accurately. Therefore, grain density measurement alone cannot be useful. Hence, other methods to resolve the charges of emitted relativistic projectile fragments have been considered. These are as follows:

(1) Blob density
(2) Gap length coefficient
(3) Mean gap length
(4) Track width
(5) Delta ray density.

Due to some limitations, none of the above methods is applicable to resolve the charges in the entire range. To estimate the charges of relativistic fragments for ^{28}Si-emulsion experiment at 3.7 A GeV, we have used blob density and gap length coefficient method for light fragments and δ-ray density measurements for heavy fragments. For light fragments, we have estimated the approximate charge of a fragment by using blob density measurements and confirmed the actual charge with the help of gap length coefficient method.

Blob density:

A blob is defined as a single grain or a set of grains merged into a clump. The blob density measurements [12] give greater reproducibility because no effort is made to resolve grains which have coalesced and it is a good parameter to resolve the charges when ionization is not very high. This method does not apply in large ionizations as the density reaches a broad maximum and then drops as blobs continue to coalesce into bigger blobs and the tracks become blacker, with just a few small gaps. The gaps then provide a measure of the ionization loss based either on their mean size or the 'linear opacity', i.e., the fraction of a track segment which is black. The related quantity is the gap length coefficient, defined by the following relation [13]:

$$B = G \exp(-\alpha G),$$

where B is the blob density, G is the gap length coefficient, and α is the parameter nearly equal to the average distance between the centres of the two crystals, which after development can be resolved in the microscope, and is determined mainly by the developed grain size and varies weakly from stack to stack.

Gap length coefficient method:

The first experimental results of the gap length coefficient measurement were reported by O'Ceallaigh [14], who found that the frequency distribution of gap lengths follows an exponential law and is applicable over a wide range of ionization. The negative slope, g, of the distribution on a log frequency vs. gap length diagram is a measure of grain density and is called the gap length coefficient. The mean gap length l is statistically equal to the reciprocal of the gap length coefficient [15]. According to the law of gap length, the density, H, of the gaps exceeding length l is given as follows [15]:

$$H = B \exp(-Gl),$$

where B is the blob density, G is the gap length coefficient and H is the number of gaps (or holes) per unit length exceeding a suitable length l measured as the distance between the inside edges of the developed grains.

For very large Z, G reaches an upper limit which is a property of the particular emulsion employed in an experiment. On plotting G for relativistic particles as a function of Z^2, Fowler and Perkins found a near proportionality till 5000/mm was reached. However, finer grains raise this limiting value. As the grain size is 0.3 μm in BR2 emulsion, excess grains are present. The grain density contributing to the gap length coefficient (G), therefore clearly exceeds the density of grains actually traversed by the ion and the corresponding value of G will be about $1/0.3\mu$, i.e., 3300/mm. In practice, the gap

length coefficient is determined by the relation: $G = 1/l(B/H)$. The following points are pertinent in the determination of G at different ionizations:

(i) For low ionizing particles, i.e., when $G\alpha < 0.35$, gap length coefficient can be determined by blob density alone.

(ii) When $G\alpha > 0.35$ (i.e., for highly ionizing particles), gap length coefficient can be measured from blob counting and by measuring the number of the gaps of certain length.

(iii) The most common gap length chosen is 2.5 times the mean gap length. With this, a high accuracy in G can be achieved. The efficiency of this method is due first, to the speed of blob counting and secondly, to the relatively small number of gaps, which can be rapidly counted without too frequent a pause for decision on borderline gap lengths. The number of large gaps to be counted generally is 1/4 the number of blobs. The statistical error in G is given by

$$\frac{\mathrm{d}G}{G} = \frac{1}{\sqrt{N_H \ln(B/H)}}, \tag{1}$$

where N_H is the number of gaps counted which have length greater than l. In order to minimize the error, we may write the above relation in the following form:

$$\mathrm{d}/\mathrm{d}H[\sqrt{H \ln(B/H)}] = 0. \tag{2}$$

On solving these equations, we get

$$\ln(B/H) = 2.0$$

or

$$B/H = 7.4.$$

The length l for different charges was selected in such a manner that the condition $4.0 \leq B/H \leq 7.0$ suggested by Fowler [15] was satisfied. For resolving different charges, we have used the blob density, gap density and the gap length coefficient method. The appropriate geometric factor for dipping tracks has been applied when necessary. However, majority of projectile fragments do not need any correction because they hardly ever dip more than 2°.

Delta ray measurement:

When an energetic heavily charged particle penetrates matter, its electric field disturbs the atomic electrons constituting collisions of varying energy transfer in which the kinetic energy of the particle is dissipated. If the kinetic energy of an electron exceeds 2 keV, its range may be enough for the formation of an electron track seen to emerge from the trajectory of the primary particle. These electron tracks are known as delta 'rays'. The number of δ-rays observed in experiments depends on the resolution as well as on the sensitivity of the emulsion.

Demers and Rossi [16,17] showed that at relativistic velocities, the energy of knock-on electrons $W_{\max}$ becomes large compared to any practical minimum δ-ray energy. So

the number of δ-rays per unit length exceeding a particular minimum energy $W_{\min}$ becomes

$$n_\delta = (2\pi r_0^2)\left(\frac{mc^2}{W_{\min}}\right) Z^2. \tag{3}$$

For a fixed choice of $W_{\min}$, $n_\delta \sim (\text{const.})Z^2$. If the constant for a particular counting convention is determined empirically for particles with known charges, then the charge of other relativistic charged particle can be estimated with good accuracy. Mathiesson [18] counted the delta rays extending from the axis of the track by 1.3μ or more. Plotting n_δ as a function of Z^2, a straight line fit was obtained with positive intercept at $Z = 0$ which was presumed to be due to the background that should be subtracted from all readings. In determining n_δ, attention was confined to δ-rays, with energy greater than about 15 keV which produce tracks with three or more grains. Tracks having energy >75 keV are generally omitted. Thus, the value of n_δ gives an approximate measure of the number of δ-rays per unit length with energy between 15 and 75 keV [19]. Frier *et al* [20] and Bradt and Peters [21] have adopted different conventions for δ-ray density measurement. However, the convention proposed by Tidman *et al* [22] is widely used. According to this convention, grain configurations to be counted as δ-rays, must attain a minimum displacement of 1.58 μm from the axis of the track projected on the plane of the emulsion. There are certain difficulties in this method as the number of δ-rays per unit length, n_δ, become large (>20) for relativistic nuclei with $Z > 14$. For higher values, one is not sure of the number of δ-rays, as the unresolved tangles become quite different. While the increased value of n_δ makes effect due to the background insignificant, it leads to increased counting errors. Therefore, counting of δ-rays is not reliable for very heavy fragments having $Z > 14$ [19].

In a sample of ^{28}Si-induced collisions, the tracks of forward-going PFs of charge greater than two were identified by the complementary measurements of the gap/blob density in terms of gap length coefficient or of the density of δ-rays over a large distance (usually a few centimeters). It was possible to visually recognize (through grain density) the $Z = 1$ and 2 PFs and therefore, systematic charge measurements were done only for PFs with $Z \geq 3$. A sample of PFs tentatively assigned $Z = 2$ was also measured and in all the cases the previous assumption turned out to be correct. Employing the gap length coefficient measurement, we were able to resolve the charges upto $Z = 6$ fragments only. The PFs with $Z > 6$ were determined by δ-ray density measurements using the following equation:

$$n_\delta = a + bZ^2, \tag{4}$$

where n_δ is the δ-ray density. The values of a and b were taken for each emulsion pellicle. Using these measurements, a calibration curve for the number of δ-rays per unit length vs. Z^2 was drawn and a straight line with positive intercept at $Z = 0$ was passed [23]. A similar curve has been reported by Barkas [13]. The above procedure yielded charge assignment to PFs covering the entire range of $Z = 1$–14 [23]. From 924 inelastic minimum-bias ($n_h \geq 0$) events, we selected 90 events with TD of the heavy emulsion (AgBr) nuclei induced by ^{28}Si nuclei based on $n_h \geq 28$ criteria. It has been found that these criteria correspond to the destruction of the nuclear emulsion target nuclei nearly to the individual nucleons with no measurable residual

nuclei existing, due to which these criteria are widely used to select the TD events of Ag(Br). For comparison, we used the data on collisions of the same incident nuclei with a lower degree of disintegration of the target or entirely used the minimum-bias events without any n_h-cut. By using these experimental data, we have analysed the dependence of the characteristics of disintegration products on the collision parameter. The experimental data also have been compared for different projectiles at the same momentum per nucleon.

3. Target identification

Nuclear emulsion is composed of different targets mainly H, C, N, O, Ag, Br and I nuclei. A clear identification of these different targets in nuclear emulsion is not so straightforward. Statistically, identification of collision events with different target nuclei in nuclear emulsion is performed on the basis of the multiplicity of heavy particles ($n_h = n_b + n_g$), which is a function of the size of the target and also is a characteristic of the impact parameter (i.e., collision centrality). On this basis, different collision events in nuclear emulsion are characterized as follows:

(1) H-events: The events which fall under the criteria $n_h \leq 1$ are collision events with hydrogen nuclei in the nuclear emulsion. These are mainly peripheral collision events.
(2) CNO-events: The events which fall under the criteria $2 \leq n_h \leq 8$ are collision events with light emulsion target nuclei C, N and O with average mass number 14. These collision events may also contain some peripheral collision events with Ag and Br nuclei. In nuclear emulsion, one cannot distinguish individual events with C, N and O on event-by-event basis. Therefore, these events are grouped together into this category with the criteria based on the n_h-value mentioned.
(3) AgBr-events: The events which fall under the criteria $n_h > 8$ are collision events with heavy target nuclei (Ag and Br nuclei) in the nuclear emulsion with average mass number 94. These events correspond to non-peripheral collision events with Ag and Br nuclei in nuclear emulsion.

In our sample of 924 minimum-bias inelastic events, the percentage of occurrence of the three different target-group events are as follows: H-group: 19.78%, CNO-group: 28.15% and AgBr-group: 52.07%.

4. The simulation

In Glauber model, the collision of two nuclei is described in terms of the individual collisions of the constituent nucleons. The MC Glauber model calculation is performed in the following manner. At first, each nucleus is stochastically determined. Then, the two nuclei are collided. Assume that the nucleons travel in a straight line along the beam axis (eikonal approximation) such that nucleons are tagged as wounded (participating) or spectator (for more details refer [24–30]). The measurement of charged nuclear fragments emitted in a narrow forward cone in the nucleus–nucleus collisions is not straightforward in a model like MC Glauber calculations, whereas, the wounded nucleon number

distribution for a sample of generated nucleus–nucleus collisions can be directly done. The forward cone of 5° for nucleus–nucleus collision at 3.7 A GeV is quite sufficient to contain all the fragments (stripped fragments of varying sizes and protons) emerged out of the projectile break-up after collision. Thus, the total charge Q of the relativistic projectile fragments in the narrow forward cone along the collision axis can be given by

$$Q = Z_{\mathrm{p}} - Q_{\mathrm{w}},$$

where Z_{p} is the projectile charge and Q_{w} is the number of wounded protons in the projectile nucleus. For the wounded nucleon calculation, we have used PHOBOS MC Glauber model as mentioned in [30].

Using the MC Glauber model code, we have simulated a sample of 10000 events separately for each target group, i.e., H target group with average mass number $A_t = 1$, CNO target group with average mass number $A_t = 14$ and AgBr target group with average mass number $A_t = 94$. These samples of 10000 generated events separately for each target group are quite sufficient to check the goodness of the data by simulation in comparison to the nuclear emulsion data where statistics is quite low due to the limitation of nuclear emulsion.

5. Total charge distributions

In minimum-bias events, along with the produced particles, the PFs also emerged in the collision process with charges varying from 1 to Z_F. As the impact parameter (b) cannot be measured directly, the measurement of charged nuclear fragments emitted in a narrow forward cone in the nucleus–nucleus collisions can provide an indirect estimation of the degree of centrality of the collision events. The experiments employing nuclear emulsions use total charge of the stripped PFs ($Q = \sum n_i Z_i$, where n_i is the number of projectile

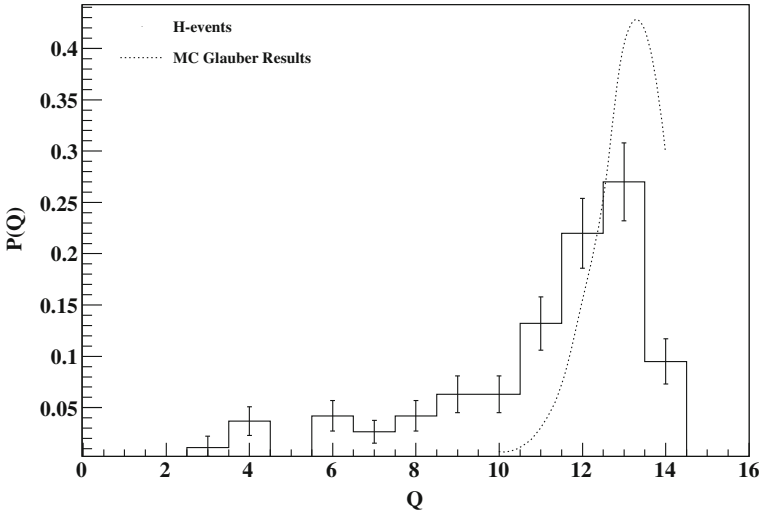

Figure 1. Total charge (Q) distribution of the projectile spectators in H-events (solid line histogram).

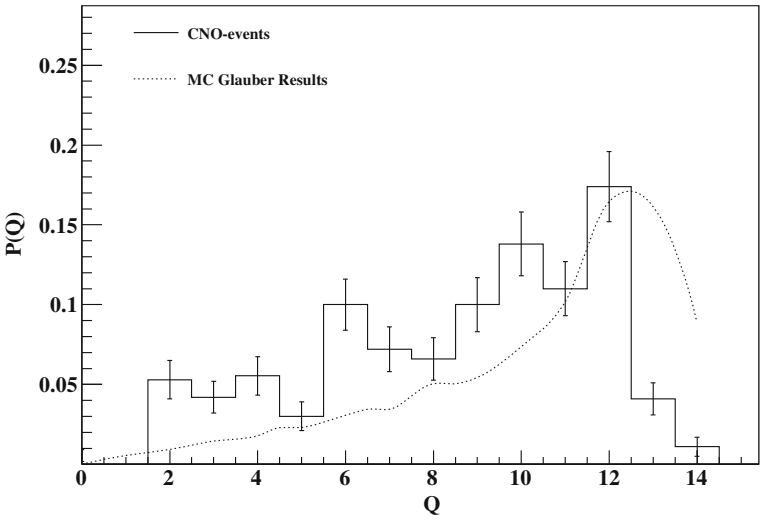

Figure 2. Total charge (Q) distribution of the projectile spectators in CNO-events (solid line histogram).

fragments with charge Z_i and summation is made over all such fragments) for this purpose. In figures 1–3, we have shown the total charge (Q) distribution of non-interacting PFs (projectile spectators) emerged in collision with different nuclear emulsion nuclei, i.e., with H-events ($n_h \leq 1$), CNO-events and AgBr-events at 3.7 A GeV. We have also compared the experimental results with MC Glauber results. In figure 1, for H-events one can see that the probability distribution of PFs charge is negligibly small upto $Q = 5$ as observed from experimental data. However, beyond $Q = 5$ it monotonically

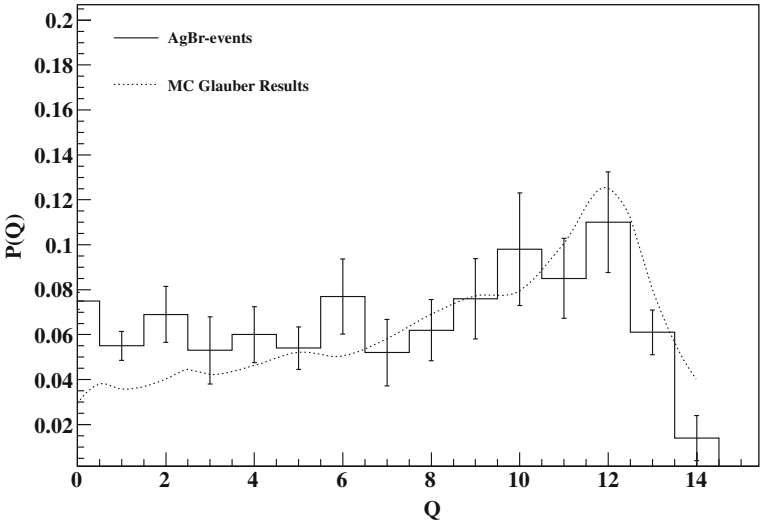

Figure 3. Total charge (Q) distribution of the projectile spectators in AgBr-events (solid line histogram).

rises upto $Q = 13$ (close to the charge Z_p of the projectile nuclei), where the peak value of the distribution is observed and then total charged distribution falls again for $Q = 14$. In this case, one can see that the curve for MC Glauber results shows a reasonable agreement with the experimental data within statistical errors only for $Q = 10$ onwards and does not extend below $Q \sim 10$. Curve for the model results overestimates the experimental results as we move towards higher Q-values.

In case of CNO-events as shown in figure 2, one can see that the probability $P(Q)$ increases with the total charge of the spectators upto $Q = 12$, where peak of the distribution is observed, after which it falls again. The low probability observed for large values of Q (>12) may be due to the contamination of some collisions with AgBr target group in the CNO-events as previously noticed by El-Nadi *et al* [31]. MC Glauber result is in reasonable agreement with the trend observed in the experimental data within statistical errors at 3.7 A GeV except for higher values of Q. Further, in the case of AgBr-events as shown in figure 3, one can see that the distribution is almost flat over a wide range of Q upto 9, after which it shows a slight increase in $P(Q)$ and again it falls for Q higher than 12. Curve for MC Glauber results shows a reasonable agreement with the experimental data. In case of AgBr-events, the lower Q side of the distribution clearly signifies the violent collision events characterizing the high temperature process [32]. These events are mainly caused by central collision events in which most of the nucleons of the projectile and the majority of the AgBr target nuclei take part in the collision [33]. We see that higher probability is observed even in the case of peripheral collisions (i.e., the higher Q side of the distribution). The MC Glauber results are in good agreement with the experimental data at 3.7 A GeV except at lower Q values, whereas MC glauber results underestimate the experimental data.

Thus, the nuclear collision events with different emulsion nuclei (i.e., H, CNO and AgBr) show that the shape of the distributions are quite different from each other and are in reasonable agreement with the model results. Furthermore, we observe that the disintegration of the projectile ^{28}Si nucleus is more severe over the entire range of Q-values in the collisions with heavy nuclei than with the lighter nuclei.

6. Characteristics of TD events for Ag and Br nuclei with varying projectile mass

From geometrical consideration, the nature of collisions can be defined by the size of the impact parameter b. In TD events (i.e., $0 < b < |R_P - R_T|$), a complete destruction of colliding nuclei takes place without emission of any spectator part of the projectile nuclei in the forward region. It is assumed that high degrees of excitation are involved in such collisions with the emission of a large number of produced particles, especially pions. The degree of target destruction (n_h) is more often used to determine the centrality of collision events in nuclear emulsion experiments. As per the criteria for TD of heavy emulsion nuclei, we have used the condition by accepting the presence of at least 28 heavily-ionizing particles (n_h) which provides the total average charge of Ag and Br ($Z = 41$). The calculated average number of participant nucleons from the beam and the target is close to 90±9.0 (maximum allowed) and there is little variation in this number when we cover the impact parameter interval 0 to $b \approx 2$ fm. One of the important characteristics of TD of Ag and Br nuclei is the probability W to be realized with different projectile

masses. This is defined as the ratio of the number of TD events to the total number of inelastic collision events involving heavy Ag and Br nuclei

$$W_{\mathrm{TD}} = \frac{N_{\mathrm{TD}}}{N_{\mathrm{Ag,Br}}}, \tag{5}$$

where $N_{\mathrm{Ag,Br}} = N_{\mathrm{inel}}/W_{\mathrm{Ag,Br}}$. The cross-section for inelastic collisions of incident ^{28}Si nuclei with emulsion nuclei are determined from the Bradt–Peters formula [34]. The values obtained for the probability of interacting with heavy emulsion components are practically identical.

In figure 4, we have shown the TD probabilities of Ag and Br for projectile nuclei of various masses at the same momentum per nucleon. We also give the results of calculations using the cascade-evaporation model [35,36]. One can observe from figure 4 that the TD probability for Ag and Br nuclei grows with increasing mass of the incident nucleus. Dubna cascade evaporation model (CEM) results overestimate the probability of this process for heavier nuclei as observed from the figure.

It may be interesting to mention that the solid line in the figure can be expressed by the following equation:

$$W(A_{\mathrm{p}}) = \beta(A_{\mathrm{p}})^{\alpha}. \tag{6}$$

The solid line is shown here to present the trend observed in the experimental data for different projectile masses. The fitting values of α and β are 2.0 ± 0.12 and 0.78 ± 0.04, respectively.

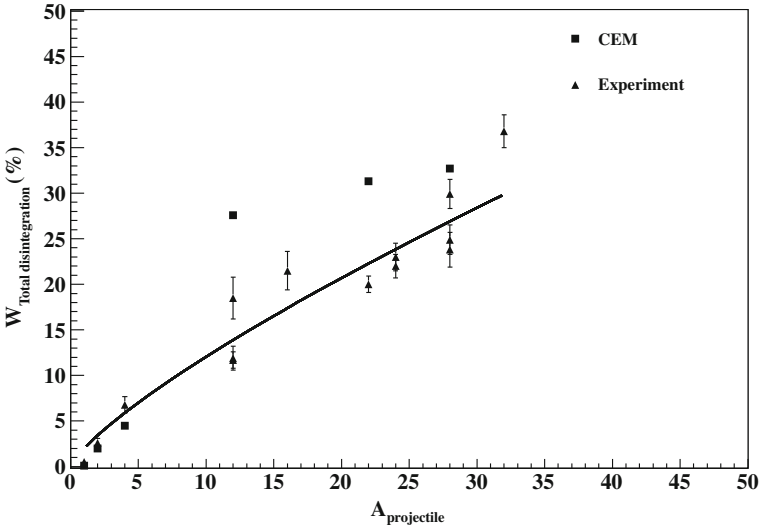

Figure 4. Probability distributions for TD events as a function of different projectile masses at the same momentum per nucleon. The results of cascade evaporation model (CEM) calculations are also given (solid square). Data are taken from [35].

7. Mean multiplicities

7.1 *Mean multiplicities in different classes of events*

The multiplicity characteristics (e.g., mean multiplicities) have been used as valuable tools to investigate the production mechanism of charged secondary particles in nucleus–nucleus collisions. In table 1, we have shown mean multiplicities of different charged secondaries (black, grey, shower particles and the projectile fragments) in minimum bias, AgBr and TD events in nucleus–nucleus collisions at 3.7 A GeV. The mean multiplicity of interacting projectile nucleons for each collision event is calculated from the experimental data using the following formula:

$$n_{\text{int}} = A_{\text{p}} - \frac{A_{\text{p}}}{Z_{\text{p}}} Q, \tag{7}$$

where A_{p} and Z_{p} are the mass number and charge of the projectile nucleus and Q is the total charge of the emanated projectile fragments which do not undergo any interactions.

Mean multiplicity of shower particles is observed to be increasing significantly with the increase in average target size (mass). Mean multiplicity of shower particles is found to be highest in the case of TD events (i.e., most central collision events with AgBr nuclei) in comparsion to the minimum-bias and AgBr events which is expected as in central collisions most of the available energy goes mainly into the production of new particles. These events represent almost 10% of the total events considered in this analysis and are extreme central collisions in which, it is assumed that almost all the projectile nucleons and a substantially large fraction of the AgBr target nucleons take part in collision [32,33,37,38]. A similar increasing behaviour is observed for the mean multiplicity of grey and black particles (i.e., mainly target fragments), which in turn results in similar behaviour of the observed mean multiplicity for heavily ionizing particles (n_{h}) (i.e., black and grey particles taken together). Further, with the increase in average target size (mass), the mean multiplicity of the projectile helium fragments ($\langle n_\alpha \rangle$) decreases substantially. Mean multiplicity of the projectile helium fragments (with charge $Z = 2$) is found to be lowest in the case of TD events in comparsion to minimum-bias and AgBr events. Mean multiplicity of the projectile helium fragments in central AgBr collisions is the lowest because majority of the projectile nucleons have participated in the initial

Table 1. The mean multiplicities of different charged secondaries for different classes of events of ^{28}Si with nuclear emulsion.

Criteria	$n_{\text{h}} \geq 0$ (min.-bias events)	$n_{\text{h}} \geq 8$ (AgBr events)	$n_{\text{h}} \geq 28$ (TD events)
N_{ev}	924	374	90
$\langle n_{\text{s}} \rangle$	15.32±0.22	24.44±1.26	34.35±3.62
$\langle n_{\text{g}} \rangle$	6.50±0.21	13.49±0.70	22.33±2.35
$\langle n_{\text{b}} \rangle$	4.32±0.14	8.38±0.43	11.36±1.20
$\langle n_{\text{h}} \rangle$	10.82±0.36	21.87±1.13	33.69±3.55
$\langle n_\alpha \rangle$	1.06±0.03	0.85±0.04	0.26±0.03
$\langle n_{\text{F}} \rangle$	0.49±0.02	0.23±0.01	0.06±0.01
$\langle n_{\text{int}} \rangle$	13.74±0.45	17.28±0.92	26.36±2.78

stage of collision resulting in the lower emission of these projectile helium fragments. A similar behaviour is also observed in the case of projectile fragments with $Z \geq 3$ in TD events in comparison with the minimum-bias and AgBr events similar to the results previously reported in [32]. On the other hand, the mean multiplicity of the interacting projectile nucleons (i.e., participating nucleons of the projectile nuclei) was found to increase substantially with increasing average target size. Highest value of $\langle n_{\text{int}} \rangle$ is observed in TD(AgBr)-events, i.e., 26.36 ± 2.78 represents nearly 94% of the projectile nucleons participating in the collision process with AgBr nuclei which indicates the maximum overlap of colliding nuclei as expected in comparison to the minimum-bias and AgBr events.

7.2 *Mean multiplicities as a function of total charge (Q) in different classes of events*

In tables 2–4, we have depicted tabular representations of variations of mean multiplicities of different charged secondaries (i.e., shower, grey, black and heavily-ionizing particles) as functions of Q in minimum-bias, CNO and AgBr events, respectively. The variation of mean multiplicity of different charged secondaries with Q-values provide us an alternative to study the significant role of centrality in the production of these charged secondaries. One can observe that the mean multiplicity of different charged secondaries in minimum-bias and AgBr events follow a decreasing trend as a function of Q-values with highest value of mean multiplicity for $Q = 0$ (i.e., most central collision events) due to the violent collision of projectile nucleus with emulsion target nuclei, whereas, in CNO-events, mean multiplicity of shower particles and grey particles show almost a decreasing trend with increasing Q-values except at $Q = 0$, where a little deviation is observed. This deviation at $Q = 0$ in CNO-events may be due to some contamination with peripheral AgBr-events, while black and grey particles in CNO-events show a saturation behaviour for $Q = 6$ and beyond.

Table 2. Variation of mean multiplicities of different charged secondaries with different Q-values in ^{28}Si-emulsion collisions (minimum-bias) at 3.7 A GeV.

Group of events	$\langle n_{\text{s}} \rangle$	$\langle n_{\text{g}} \rangle$	$\langle n_{\text{b}} \rangle$	$\langle n_{\text{h}} \rangle$
$Q = 0$	36.19±4.39	18.72±2.27	8.56±1.04	27.28±3.30
$Q = 1$	35.82±5.06	18.64±2.64	9.68±1.37	28.32±4.00
$Q = 2$	26.32±3.72	11.98±1.69	7.46±1.06	19.44±2.74
$Q = 3$	25.21±3.68	10.57±1.54	6.47±0.94	17.04±2.49
$Q = 4$	21.31±2.90	9.48±1.29	6.26±0.85	15.74±2.14
$Q = 5$	18.27±2.85	6.41±1.00	4.22±0.66	15.74±2.14
$Q = 6$	15.77±1.88	6.29±0.75	5.27±0.63	11.56±1.38
$Q = 7$	14.86±1.97	4.84±0.65	3.46±0.46	8.35±1.10
$Q = 8$	12.25±1.62	4.84±0.64	4.32±0.57	9.16±1.21
$Q = 9$	10.43±1.25	3.97±0.47	3.53±0.42	7.36±0.88
$Q = 10$	8.13±0.86	2.94±0.31	2.87±0.30	5.81±0.61
$Q = 11$–14	3.36±0.24	1.64±0.10	1.61±0.10	3.25±0.21

Table 3. Variation of mean multiplicities of different charged secondaries with different Q-values in ^{28}Si-CNO collisions at 3.7 A GeV.

Group of events	$\langle n_s \rangle$	$\langle n_g \rangle$	$\langle n_b \rangle$	$\langle n_h \rangle$
$Q = 0$	17.00±9.88	4.33±2.80	0.67±0.40	5.00±3.20
$Q = 1$	28.00±15.70	5.00±2.88	2.00±1.15	7.00±4.03
$Q = 2$	22.78±7.59	2.67±0.89	1.78±0.59	4.40±1.46
$Q = 3$	22.25±6.42	3.58±1.03	1.83±0.53	5.42±1.24
$Q = 4$	18.93±5.06	3.00±0.80	1.43±0.38	4.43±1.18
$Q = 5$	17.32±3.69	3.09±0.66	1.64±0.34	4.73±1.01
$Q = 6$	14.75±2.61	3.09±0.55	1.94±0.34	5.03±0.89
$Q = 7$	13.10±2.39	2.80±0.51	2.10±0.38	4.90±0.89
$Q = 8$	10.59±1.97	2.24±0.41	2.38±0.44	4.62±0.85
$Q = 9$	9.60±1.62	2.31±0.39	2.43±0.41	4.46±0.80
$Q = 10$	7.35±0.99	2.29±0.31	2.31±0.31	4.58±0.62
$Q = 11$–14	5.77±0.55	2.14±0.20	2.46±0.23	4.60±0.43

8. Pseudorapidity distribution of relativistic charged particles

In high-energy collisions, one of the fundamental experimental observables which is generally compared with any successful theoretical model is the pseudorapidity ($\eta = -\ln\tan(\theta/2)$) distribution of the produced shower particles. Pseudorapidity density is also an important quantity to get information on the temperature and energy density of the nuclear matter formed during the collision [39–41]. In figure 5, we have shown the pseudorapidity distributions of shower particles induced by ^{28}Si nuclei for minimum-bias as well as central collision events. It is clearly observed from figure 5 that the average multiplicity of shower particles per η bin in TD events is higher relative to the minimum-bias events both in the midrapidity as well as target fragmentation regions, while in projectile

Table 4. Variation of mean multiplicities of different charged secondaries with different Q-values in ^{28}Si-AgBr collisions at 3.7 A GeV.

Group of events	$\langle n_s \rangle$	$\langle n_g \rangle$	$\langle n_b \rangle$	$\langle n_h \rangle$
$Q = 0$	38.84±4.93	20.32±2.58	9.35±1.18	29.68±3.77
$Q = 1$	35.98±5.14	18.92±2.70	9.84±1.40	28.76±4.10
$Q = 2$	26.65±3.81	14.63±2.09	9.78±1.40	27.24±3.89
$Q = 3$	24.83±4.20	12.60±2.13	7.94±1.34	21.62±3.65
$Q = 4$	22.42±3.74	13.0±2.16	8.83±1.47	21.83±3.64
$Q = 5$	17.30±3.33	8.44±1.62	5.85±1.12	14.30±2.75
$Q = 6$	17.66±3.12	10.66±1.88	9.56±1.68	20.22±3.58
$Q = 7$	17.00±3.80	9.60±2.15	6.55±1.46	16.15±3.60
$Q = 8$	15.05±3.20	9.09±1.94	7.59±1.62	17.54±3.74
$Q = 9$	13.00±2.84	8.81±1.92	7.43±1.62	16.24±3.54
$Q = 10$	9.7±2.16	6.70±1.50	6.35±1.42	13.05±2.92
$Q = 11$–14	10.94±3.44	9.33±2.90	5.76±1.77	14.95±4.63

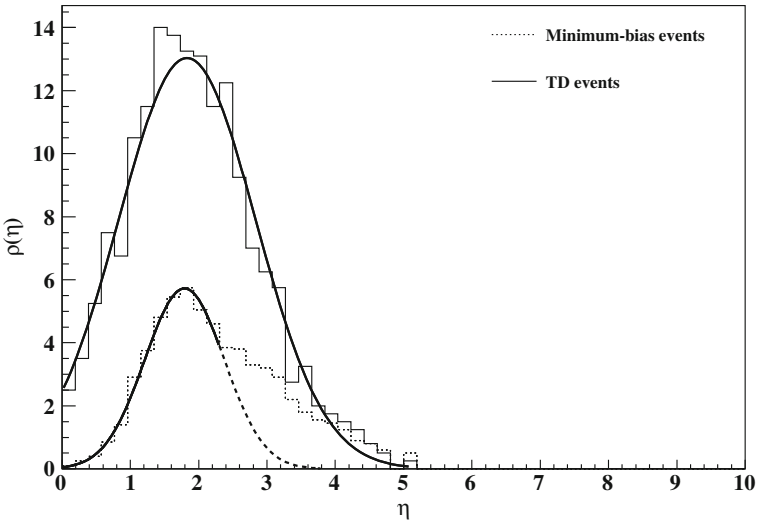

Figure 5. Pseudorapidity distributions of shower particles produced in ^{28}Si-emulsion collisions for minimum-bias and TD events.

fragmentation region, the corresponding value per η bin remains more or less comparable to the minimum-bias events. Pseudorapidity density distribution of shower particles for TD events is well described by the Gaussian function, whereas in the case of minimum-bias events, distribution follows the Gaussian form upto $\eta = 2.15$, but for higher values of η, deviation is clearly visible in the form of asymmetric distribution in the projectile fragmentation region. This observed asymmetry of distribution in the projectile fragmentation region may be due to the high contributions of H- and CNO-events which is reflected in the form of assymmetrical distribution with extended tail reflecting a clear shift from Gaussian distribution as observed in TD events.

To further investigate these features of TD events, we examine the normalized pseudorapidity density $R(\eta)$ in greater detail. $R(\eta)$ can be defined as

$$R(\eta) = \frac{\rho_x(\eta)}{\rho_{nh=0,1}(\eta)}, \tag{8}$$

where $\rho(\eta) = (1/N)(\mathrm{d}N_\mathrm{s}/\mathrm{d}\eta)$ is the shower particle density determined for N collisions. The term $\rho_x(\eta)$ denotes the pseudorapidity density either in TD or in minimum-bias events. The term $\rho_{nh=0,1}(\eta)$ is the particle density of shower particles produced in H-events (i.e., Si–H collisions) in nuclear emulsion and serves the purpose in similar way to that of the proton–nucleus collisions at the same projectile energy in nuclear emulsion. $\rho_{nh=0,1}(\eta)$ is obtained by selecting the H-events falling under the criteria $n_\mathrm{h} \leq 1$. Thus, the parameter $R(\eta)$ roughly signifies the number of interacting nucleons in the projectile nucleus [42,43]. The normalized pseudorapidity densities $R(\eta)$ for both TD and minimum-bias events are shown in figure 6. One can observe from figure 6 that the normalized pseudorapidity density is less than one in the projectile fragmentation region for both types of events ($\eta \sim 2.4$ onwards). In turn, this would indicate that the additional particles created in consecutive intranuclear collisions take away some

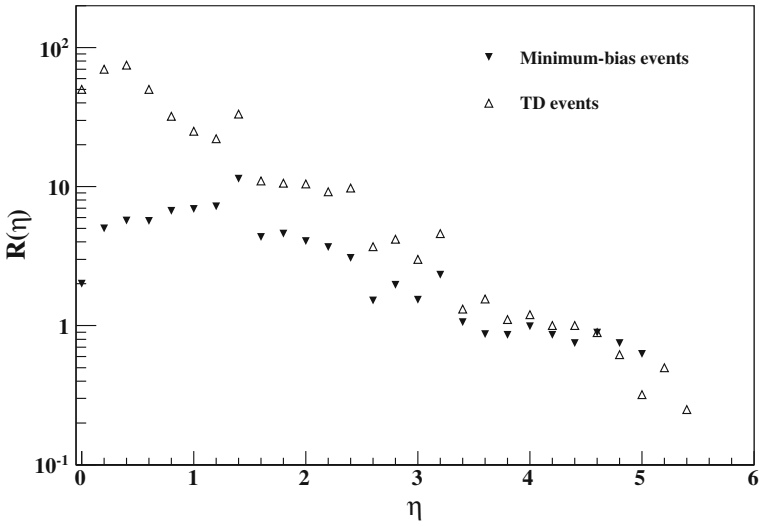

Figure 6. Normalized pseudorapidity density $R(\eta)$ for minimum-bias events (solid triangle) and TD events (open triangle).

of the energy of the projectile nucleus thereby reducing its momentum as compared to the peripheral collisions. The normalized pseudorapidity density increases rapidly for TD events in the target fragmentation region ($0 < \eta < 1.2$) in comparison to minimum-bias events.

9. Summary and conclusion

The extensive analysis of the experimental data of ^{28}Si nuclei with different emulsion target groups at 3.7 A GeV was performed to study the nuclear fragmentation properties and the underlying mechanism of particle production. These experimental results have been compared with the calculations based on MC Glauber model. Further, we have studied the pseudorapidity and normalized pseudorapidity distributions of shower particles produced in nucleus–nucleus collisions at 3.7 A GeV. From this extensive analysis, we conclude this research paper with the following important observations:

The total charge distributions of projectile fragments emerged out of the nuclear collisions with different target nuclei are qualitatively supported by MC Glauber calculation results. The fragmentation property of the projectile ^{28}Si nucleus depends strongly on the target size as observed in the total charge distribution for different target groups. The PFs with relatively higher charge are most abundant in collisions with the light (H) and intermediate (CNO) target nuclei, whereas a noticeable enhancement in the yield of PFs with smaller charge is clearly visible in collisions with the heavy target nuclei (AgBr). This type of behaviour clearly indicates the significant role of the impact parameter in fragmentation mechanism. The TD probability of these nuclei grows with increasing size of the projectile nuclei whereas CEM calculation overpredicts the experimental results for the collision events of projectile nuclei with larger mass. The results obtained reveal that the

probability of TD of AgBr target nuclei strongly depends on the projectile mass. Mean multiplicity of relativistic shower particles, target fragments and interacting nucleons produced in TD events increases rapidly in comparison with other inelastic processes such as minimum-bias events and the events with AgBr ($n_h > 8$), while PFs (with $Z \geq 2$) show an opposite behaviour. The trend of pseudorapidity distribution of shower particles in TD events is well described by the Gaussian distribution with width σ, whereas in minimum-bias events a clear departure from the Gaussian distribution is observed, which is mainly due to the intermixing of other target groups (i.e., H- and CNO-events). The normalized pseudorapidity density $R(\eta)$ exhibits a similar variation with η throughout the pseudorapidity range for both minimum-bias and TD events. The observed high values of normalized shower particle densities in the target fragmentation region can be explained on the basis of the occurrence of some cascading effects inside the target nucleus due to some secondary collisions of low-energy pions produced in the η region.

Acknowledgement

Ashwini Kumar sincerely acknowledges the Council of Scientific and Industrial Research (CSIR), New Delhi for providing a research grant. BKS is thankful for DST and ISRO-SSPS grant.

References

[1] C P Singh, *Phys. Rep.* **236**, 147 (1993)
[2] H Satz, *Rep. Prog. Phys.* **63**, 1511 (2000)
[3] J Kapusta, P Lichard and D Seibert, *Phys. Rev. D* **44**, 2774 (1991)
[4] E V Shuryak, *Phys. Lett. B* **78**, 150 (1978)
[5] Ashwini Kumar, B K Singh, P K Srivastava and C P Singh, *Eur. Phys. J. Plus* **128**, 15 (2013)
[6] Ashwini Kumar, P K Srivastava, B K Singh and C P Singh, *Adv. High Energy Phys.* **2013**, 352180 (2013)
[7] Wang Er-Qin, *Chin. Phys. Lett.* **28** 082501 (2011)
[8] B K Singh, I D Ojha and S K Tuli, *Nucl. Phys. A* **570**, 819 (1994)
[9] Ashwini Kumar, G Singh and B K Singh, *J. Phys. Soc. Jpn* **81**, 044201 (2012)
[10] Ashwini Kumar, G Singh and B K Singh, *J. Phys. Soc. Jpn* **81**, 124202 (2012)
[11] B K Singh and S K Tuli, *Int. J. Mod. Phys. E* **7**, 341 (1998)
[12] M M Shapiro, *Encyclopedia of physics* edited by S Flugge (Springer, Berlin, 1958) Vol. XLV, p. 352
[13] W H Barkas, *Nuclear research emulsion*, Part I (Academic Press, New York, 1963)
[14] C O'Ceallaigh, *Nuo. Cim. Suppl.* **12**, 412 (1954)
[15] P H Fowler and D H Perkins, *Phil. Mag.* **46**, 587 (1955)
[16] P Demers, *Ionographie* (Univ. Montreal Press, Montreal, 1958)
[17] B Rossi, *High energy particles* (Prentice Hall Inc., New York, 1952) p. 24
[18] O Mathiesson, *Arkiv. Fysik.* **17**, 441 (1960)
[19] P Powell, F Fowler and D H Perkins, *A study of elementary particles by photographic method* (Pergamon Press, London, 1959)
[20] P Frier *et al*, *Phys. Rev.* **74**, 1828 (1948)
[21] H L Bradt and B Peters, *Phys. Rev.* **74**, 1828 (1948)
[22] D A Tidman, E P George and A J Herz, *Proc. R. Soc. A* **66**, 1019 (1953)
[23] B K Singh, Ph.D. Thesis (Banaras Hindu University, Varanasi, India, 1995)

[24] M L Miller, K Reygers, S J Sanders and P Steinberg, arXiv:nucl-ex/0701025 (2007)
[25] PHOBOS Collaboration: B Alver *et al, Phys. Rev. C* **77**, 014906 (2008), arXiv:0711.3724 [nucl-ex]
[26] H De Vries, C W De Jager and C De Vries, *At. Data Nucl. Data Tables* **36**, 495 (1987)
[27] L Hulthen and M Sugawara, *Handbuch der Physik* **39**, 1 (1957)
[28] PHENIX Collaboration: S S Adler *et al*, *Phys. Rev. Lett.* **91**, 072303 (2003)
[29] See http://root.cern.ch for installation and documentation
[30] See the TGlauberMC page on HepForge (http://www.hepforge.org/downloads/tglaubermc) for the most recent TGlauberMC release
[31] M El-Nadi *et al*, *J. Phys. G: Nucl. Part. Phys.* **24**, 2265 (1998)
[32] M A Jilany, *Phys. Rev. C* **70**, 014901 (2004)
[33] B K Singh and S K Tuli, *Nucl. Phys. A* **602**, 487 (1996)
[34] H L Bradt and B Peters, *Phys. Rev.* **91**, 54 (1950)
[35] N N Abd-Allah, *Phys. Scr.* **47**, 501 (1993)
[36] V S Barashenkov, F G Zheregi and Zh Zh Musalmanbekov, JINR Preprint, Dubna, 1983, 283
[37] B K Singh and S K Tuli, *Nuovo Cimento Soc. Ital. Fis. A* **112**, 1093 (1999)
[38] M M Sherif, M A Jilany, M N Yasin and S M Abd-Elhdin, *Phys. Scr.* **51**, 431 (1995)
[39] X N Wang and M Gyulassy, *Phys. Rev. Lett.* **86**, 3496 (2001)
[40] A Capella and D Sousa, *Phys. Lett. B* **511**, 185 (2001)
[41] K J Eskola, K Kajantie, P V Ruuskanen and K Tuominen, *Nucl. Phys. B* **570**, 379 (2000)
[42] S A Azimov *et al, Nucl. Phys. A* **470**, 653 (1987)
[43] T Ahmad, M A Nasr and M Irfan, *Phys. Rev. C* **47**, 2974 (1993)